Materials Advances

ROYAL SOCIETY OF CHEMISTRY

PAPER

View Article Online
View Journal | View Issue

Cite this: *Mater. Adv.*, 2022, 3, 6619

Solution-processed linear methyl methacrylate-*co*-glycidyl methacrylate films with excellent dielectric and energy storage characters†

Junhao Xie,[a] Hongxu Liu,[a] Jing Hu,[a] Xuanchen Zhao,[a] Shixin Song,[b] Shulin Sun *[a] and Mingyao Zhang*[a]

Received 20th April 2022,
Accepted 13th July 2022

DOI: 10.1039/d2ma00437b

rsc.li/materials-advances

Research on linear dielectric glass polymer films with high permittivity and low loss has attracted much attention recently. In the present report, a series of methyl methacrylate (MMA) and glycidyl methacrylate (GMA) copolymers (MG) with different MMA/GMA ratios were synthesized by a continuous solution polymerization and devolatilization extrusion method and their corresponding MG dielectric films were prepared *via* a solution-processed method. Different from the pristine poly MMA (PMMA) film, the introduction of GMA endowed higher polarity and provided deep traps. Consequently, the MG films demonstrated higher permittivity (5.5–7.0, 100 Hz) and lower loss than the pristine PMMA films. Moreover, the improved Young's modulus and low dielectric/conductive loss led to a higher Weibull breakdown strength of the MG films (450–530 MV m^{-1}). The excellent dielectric performance and breakdown resistance allowed achieving superior energy storage properties for the MG dielectric films. In particular, the discharged energy density and charge–discharge efficiency reached 6.81 J cm^{-3} and 84.1% at 500 MV m^{-1} for the MG 8 film. Therefore, this research provides a new dielectric polymer material with good cost performance, which displays potential application prospects in the thin-film capacitor field.

Introduction

With the rapid development of global energy resources in past few decades, the research on energy storage devices has drawn widespread concern. As one of the important energy storage devices, capacitors play a vital role in the advanced electrical and electronic industries.[1–8] According to reports, the much-needed energy density of the capacitor is mostly determined by the dielectric materials between the two electrodes. The energy density (U) can be defined as

$$U = \int EdD \quad (1)$$

where E is the applied electric field and D represents the electric displacement.[9] For linear dielectrics, it can be derived from the following formula:

$$U = 1/2\varepsilon\varepsilon_0 E_b{}^2 \quad (2)$$

where ε is the dielectric constant, ε_0 is the vacuum permittivity (8.85×10^{-12} F m^{-1}), and E_b is the dielectric breakdown strength.[6] One can see from the formula that U is determined by the dielectric constant (ε) and breakdown strength (E_b). Furthermore, compared with ε, the contribution of E_b on energy density is greater due to their quadratic relationship.

At present, biaxially oriented polypropylene (BOPP)- and ferroelectric poly (vinylidene fluoride) (PVDF)-based polymer films are the two main types of commonly used dielectric capacitor materials. The state-of-the-art BOPP capacitor film has a low dielectric loss (<0.0002 at 1 kHz), ultrahigh E_b (700–800 MV m^{-1}), and perfect discharging efficiency of almost 100%. However, the non-polar BOPP film merely shows a low energy density below 3–4 J cm^{-3} due to its low dielectric permittivity of ε = 2.2, even in different electric fields,[3,8,10] which leads to a large volume fraction of the capacitor in power delivery systems, which is useful to enhance the energy load. The bulky capacitor dimensions incur higher requirements for the assembly and reliability of power systems, especially under the trend for device miniaturization. Therefore, developing new polypropylene (PP)-based dielectric polymers with high energy density has become particularly important. For example, Chung[11] *et al.* fabricated a series of PP copolymers with different contents of -OH side groups. The H-bonding of the inter-chain –OH groups could not only form a unique and stable network

[a] *Engineering Research Center of Synthetic Resin and Special Fiber, Ministry of Education, Changchun University of Technology, Changchun 130012, China. E-mail: sunshulin1976@163.com*
[b] *School of Food Science and Engineering, Jilin Agricultural University, Changchun 130012, China*

† Electronic supplementary information (ESI) available. See DOI: https://doi.org/10.1039/d2ma00437b

architecture but also afforded a high crystallinity. Thus, the PP copolymers obtained a high polarizability and good reversibility, which resulted in a high discharging energy density beyond 7 J cm^{-3} without any significant energy loss in an electric field of 600 MV m^{-1}. Based on this research, they also produced a new polypropylene-hindered phenol copolymer (PP–HP) by Steglich esterification from the PP–OH.[12] The PP–HP copolymer showed similar dielectric properties as PP–OH but better thermal stability, which allow it to be used in harsh environmental conditions. However, the complex molecular design and polymerization mechanism of the reported PP copolymers make it difficult to replace the commercial BOPP dielectric film.

The dielectric and energy storage properties based on ferroelectric PVDF and its copolymers have been studied extensively over the past two decades.[1,13–19] The outstanding advantages of these materials lie in their strong dipole moment from the C–F bonds, which results in a high dielectric permittivity (10–50) and breakdown strength ($\sim$700 MV m^{-1} for capacitor grade films). Furthermore, due to their semi crystalline essence, these fluororesin-based capacitor films can be produced according to the manufacturing principles for commercial BOPP. Nonetheless, owing to the intrinsic dipole coupling, ferroelectric losses, large remnant polarization, and hysteresis still exist. This means that PVDF-based ferroelectric dielectrics cannot be directly applied in AC conditions due to their significantly decreased discharged energy density and low energy efficiency, especially in high electric fields. In order to overcome the disadvantages and promote the applications of these ferroelectric PVDF-based materials in the dielectric capacitor field, some strategies, such as bulky-monomer copolymerization, grafting modification, irradiation-induced crosslinking, and stretch orientation, have been utilized to suppress the cooperative ferroelectricity in the crystals zone.[20–23] Though these approaches have obtained different achievements, the high cost and complicated polymerization or modification process still seriously limit their large-scale practical applications.

Based on the above considerations, a linear dielectric of a polar polymer with a high dielectric constant and strong breakdown resistance should be an ideal choice as the capacitor film. According to this standard, polar poly(methyl methacrylate) (PMMA) and its copolymers film should be more appropriate due to its excellent mechanical properties, strong polarity, thermal stability, high glass transition temperature, and suitable price cost.[24] As a comparison, PMMA exhibits higher permittivity and breakdown strength than pristine PP. Compared with PVDF, PMMA has a lower dielectric loss, and higher E_b and energy efficiency due to the lack of polarization hysteresis. Recently, the dielectric and energy storage properties of PMMA-based films have been reported in some research studies utilizing copolymerization and nanocomposite regulation methods. For example, Zhang's group prepared poly(methyl methacrylate-methallyl alcohol) (P(MMA-MAA)) copolymer dielectric films and investigated their energy storage properties. The -OH groups on MAA formed H-bonds between the -OH and ester groups, leading to a higher T_g and modulus of the P(MMA-MAA) films. A maximum discharged energy density of 13 J cm^{-3} was achieved, which was 2–3 times higher than for BOPP.[25] Cheng and co-workers used $Ba_{0.5}Sr_{0.5}TiO_3$ (BST) nanoparticles to improve the dielectric and energy storage properties of PMMA.[26] The results showed that the PMMA nanocomposite film had a high dielectric constant and low dielectric loss with 30 vol% BST addition. Hence, a high energy storage density of more than 11 J cm^{-13} was achieved.

Compared with the above methods, the present research provides a simpler and large-scale preparation strategy for PMMA copolymers by a continuous polymerization and devolatilization extrusion method. In this paper, a series of MMA and glycidyl methacrylate monomer (GMA) copolymers (MG) were synthesized with different MMA/GMA ratios. On the one hand, the GMA monomer has higher polarity than MMA due to the presence of an epoxy group in the GMA; therefore the MG copolymers show a higher dielectric constant than PMMA. On the other hand, the epoxy group in the GMA provides reactive sites for later modifications, such as crosslinking and interfacial design, for MG-based composites. The MG films were manufactured by a simple solution-casting method and the dielectric and energy storage properties of the MG dielectric films were studied in depth. The deep energy traps provided by GMA led to a reduction in the leakage current and a low dielectric loss. Concurrently, a maximum discharged energy density of 6.81 J cm^{-3} was achieved, together with an efficiency of 84% at 500 MV m^{-1} for the MG 8 film, which was 72% higher than the discharged energy density of the pristine PMMA film. Also, the MG copolymer can be mass-produced due to its good cost performance and easily synthetic method, which endow the MG films with favorable prospects as a new commercial capacitor dielectric film material.

Experimental section

Materials

MMA and toluene were kindly provided by Jilin Petrochemical Company, China. Glycidyl methacrylate monomer (GMA) was bought from Mitsubishi Group, Japan. *N*,*N*-Dimethylformamide (DMF) was purchased from Beijing Chemical Reagent Company, China. Reagent grade initiator di-*tert*-butyl peroxide (DTBP) was bought from Alfa Aesar.

Preparation of MG copolymers

A continuous solution polymerization and devolatilization extrusion method was utilized to prepare MG copolymers. First, an MMA/GMA/toluene/initiator mixture was pre-filled in the reactor to two-thirds of the volume. The polymerization formulas for the PMMA and MG copolymers are listed in Table S1 (ESI†). After that, the mixture was heated to 150 °C in an oil bath. When the polymerization reached steady state, the reaction mixture was injected into the reactor by the feed pump at a continuous rate, and simultaneously, the reaction product was successively transported into the devolatilization extruder by a melt pump at the same feed speed to remove the

Table 1 Compositions of the MG copolymers

Designation	MMA content in monomers (wt%)	GMA content in monomers (wt%)	GMA molar ratio in monomers (mol%)	GMA molar ratio in MG copolymers (mol%)
PMMA	100	0	0	0
MG 4	96	4	2.8	2.2
MG 8	92	8	5.8	5.3
MG 12	88	12	8.8	8.2

residual monomer and solvent. Finally, the obtained MG copolymers were cooled, pelletized, and dried for film preparation.

The compositions of the MG copolymers are given in Table 1. The detailed calculation process for the GMA relative molar ration in the MG copolymers is provided in the supporting information. The setup used for the MG copolymers preparation and the schematic chemical structure of the copolymers are illustrated in Fig. 1 and 2, respectively.

Fabrication of the films

First, 1 g PMMA or MG copolymers was separately added into 10 ml DMF and stirred vigorously for 12 h at 60 °C until clear solutions were obtained. After that, the solutions were cast into membranes on a clean glass substrate at 60 °C in a vacuum environment for 12 h to remove the solvent completely. The films were peeled off from the substrates in DI water and dried for an additional 12 h at 60 °C in a vacuum. The thickness of the membranes was controlled at 20 μm.

Characterization

The ^{1}H NMR spectra of the PMMA and MG copolymers were obtained using a 400 MHz nuclear magnetic resonance (NMR) spectrometer (Bruker Instruments, model Advance III 400, Germany) at room temperature with $CDCl_3$ as the solvent and

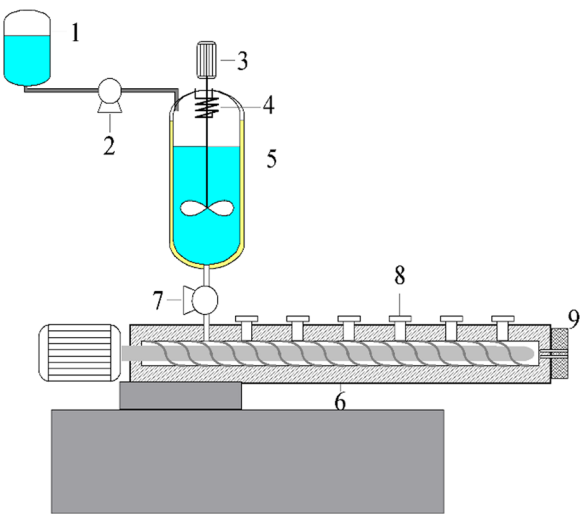

Fig. 1 Schematic of the continuous polymerization and devolatilization extrusion setup: (1), premixing tank; (2), injection pump; (3), stirring motor; (4), gas condensing tubes; (5), reactor; (6), devolatilization extruder; (7), melt pump; (8), volatilization mouth; (9), extruder die.

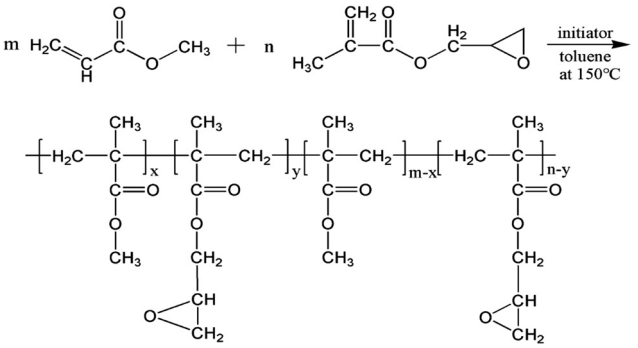

Fig. 2 Reaction pathway and chemical structure of the MG copolymers.

TMS as the internal standard. Fourier transform infrared spectroscopy (FTIR, Thermo Nicolet Avatar-360 spectrometer) was carried out to confirm the chemical compositions of the PMMA and MG in the range of 4000–400 cm^{-1}. A dynamic mechanical analyzer (DMA, PerkinElmer) was used to test the glass transition temperature (T_g) in the temperature range from 30 °C to 180 °C with a heating rate of 3 °C min^{-1}. Differential scanning calorimetry (DSC) was performed on a 1 STARe instrument (Mettler Toledo) to check the thermal properties at a heating and cooling rate of 10 °C min^{-1}. The samples were first heated from 30 °C to 220 °C to remove the thermal history and then cooled to 30 °C again. Afterwards, the samples were heated a second time to 220 °C, during which time a stable temperature was maintained for 5 min at the end of each program segment. The data from the second heating steps were used for the thermal analysis. Optical transmittance spectra were obtained on a UV-vis spectrophotometer (Agilent Cary 5000, USA) within the range of 200–800 nm. The thickness of the samples for the optical transmittance tests was about 0.1 mm. The dielectric performances were tested by using an LCR meter (E4980A, Keysight Technologies, USA) under the frequency range of 10^2–10^6 Hz. All the samples were coated with silver electrodes on both surfaces before the measurements. The polarization–electric field (*P*–*E*) hysteresis loops of the samples were measured with a ferroelectric test system (CPE1901, Polyk) at 100 Hz at room temperature. The dielectric breakdown strength measurements also used the same instrument as used to measure the *P*–*E* loops at a direct-current voltage ramp of 500 V^{-1} s^{-1}. The Young's modulus tests were carried out on an Instron 3365 tensile machine with an extension rate of 50 mm min^{-1} under 23 °C.

Results and discussion

Characterization of the MG copolymers

In order to prove the successful copolymerization of MMA and GMA, the test results from the ^{1}H NMR and FTIR characterizations of the PMMA and MG copolymers are provided in Fig. 3. It can be clearly seen from Fig. 3a that, different with the pristine PMMA, three new peaks appeared at 2.66, 2.87, and 3.23 ppm for the MG copolymers, which were in agreement with the H characteristic displacement peaks on the epoxy group of GMA. The FTIR spectra

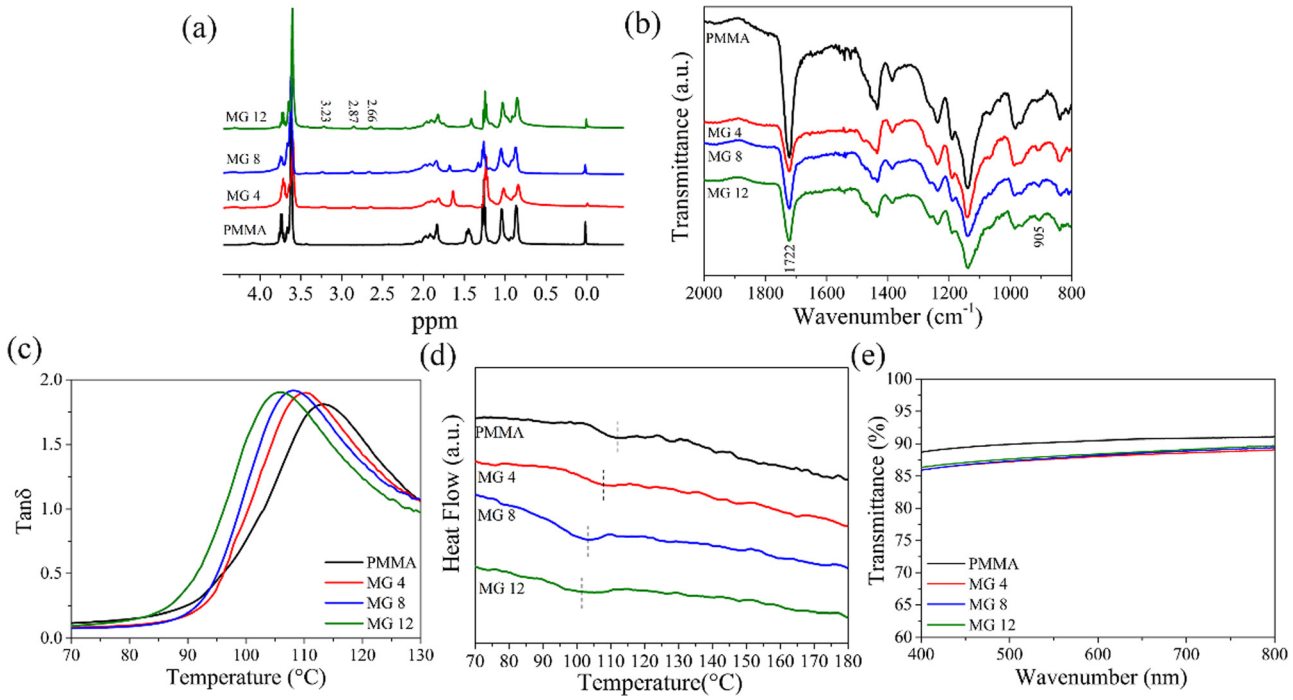

Fig. 3 ^{1}H NMR (a), FTIR (b), DMA (c), DSC curves during the heating cycle (d), and optical transmittance (e) of the PMMA and MG copolymers.

of PMMA and MG copolymers are provided in Fig. 3b. Compared with the pristine PMMA, a new absorption peak at 905 cm^{-1} was noted, corresponding to the epoxy group of GMA in the MG copolymer. The ^{1}H NMR and FTIR results verified the MG copolymers had been successfully prepared.

The influence of the MMA/GMA composition on the glass transition temperature (T_g) of MG films can be seen in Fig. 3c. Compared with PMMA (113 °C), the introduction of GMA made the T_g of MG move to a lower temperature, namely 110 °C, 108 °C, and 105 °C for the MG4, MG8, and MG12 films. This can be explained as due to the copolymerization of GMA in MG, which increased the distance between the molecular chains due to the bigger volume of GMA; therefore, the interaction between the chains became weak and the T_g of MG decreased. DSC was also utilized to determine the accuracy of the T_g, as shown in Fig. 3d. It was found that the pristine PMMA showed a T_g (112 °C) similar to the DMA result. A similar trend to DMA could be seen with increasing the GMA content, *i.e.*, the T_g decreased with increasing the GMA content, corresponding to 107 °C for MG4, 103 °C for MG8, and 101 °C for MG12, respectively. The experimental results were in agreement with the above DMA results. Although the T_g decreased with the GMA content, which still remained at 101–105 °C for the MG12 film, the high T_g of MG is beneficial for a low loss for the dielectric films under a high electrical field. Optical transmission is another critical element for energy storage films, so that they can be more widely applied in a range of applications due to their good optical transmission. Fig. 3e illustrates the optical transmission of the PMMA and MG films from 200 nm to 800 nm wavenumbers. It is evident from the diagram that pure PMMA had the highest

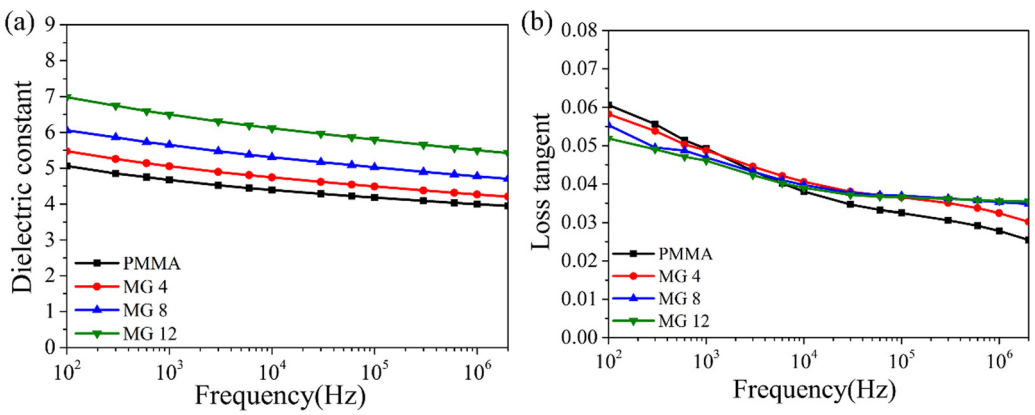

Fig. 4 Frequency dependence of the dielectric constant (a) and dielectric loss (b) of the PMMA and MG films.

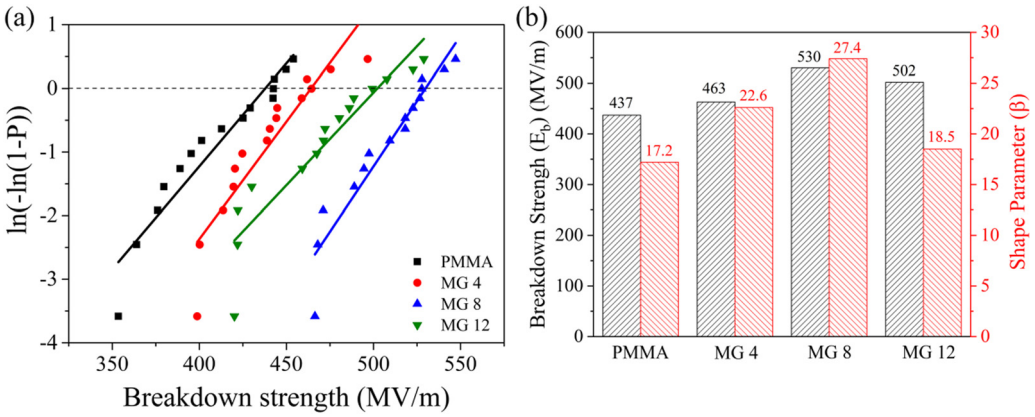

Fig. 5 Weibull distribution curves (a) and breakdown strength and shape parameters (b) of the PMMA and MG films.

optical transmission of 89.9% at 800 nm. When GMA was introduced, the optical transmission decreased slightly, namely to 87.2%, 87.3%, and 87.6% for MG4, MG8, and MG12, respectively. These results suggest that the MG films also possessed good optical transmittance comparable to PMMA.

Dielectric constant and dielectric loss

In order to demonstrate the dielectric properties of the MG copolymers compared to PMMA, the frequency-dependent dielectric constant and dielectric tangent loss ($\tan\delta$) were investigated. It can be seen from Fig. 4a that the dielectric constant value increased with the content of GMA in the wide frequency range from 10^2 to 10^6 Hz (PMMA < MG4 < MG8 < MG12). For example, the MG 12 film had a high permittivity of 6.98 compared to PMMA and PP at 10^2 Hz, which was nearly 40% higher than PMMA and more than three times higher than PP. Comparing the molecular structures of the MMA and GMA monomers, it can be seen that the GMA has an extra polar epoxy group; therefore, the copolymerization of GMA increases the polarity and dielectric constant of MG films. A similar conclusion has been reported in other research studies.[27,28] At the same time, the $\tan\delta$ values of the MG films showed a decreasing trend with the increase in GMA content at low frequencies ($<10^4$ Hz). The lower dielectric loss of MG films at low frequency is likely due to the introduction of charge traps, which limit the leakage current and thus reduce the conduction loss. On the other hand, the loss tangent of MG films exceeded that of the PMMA film by a little degree when the frequency was higher than 10^4 Hz, because of the relaxation of the GMA group at high frequencies. In general, the introduction of GMA improves the dielectric constant while maintaining a low dielectric loss for MG films.

Weibull breakdown strength

It can be determined from eqn (1) and (2) that a high dielectric breakdown strength is even more effective to achieve high energy densities rather than just possessing a high dielectric constant. The dielectric breakdown strength of the PMMA and the MG films was inspected with the two-parameter Weibull distribution, which can be calculated according to the follow equation:

$$P(E) = 1 - \exp\left((-E/E_b)_\beta\right) \quad (3)$$

where $P(E)$ is the cumulative probability of electrical failure, E is the experimental breakdown strength, E_b is the characteristic breakdown strength, which represents the sample has a cumulative failure probability of 63.2% at this electric field, and β is the shape parameter representing the degree of dispersion of the data.[29,30] As shown in Fig. 5a, among all the samples, the MG 8 film had the greatest dielectric breakdown strength.

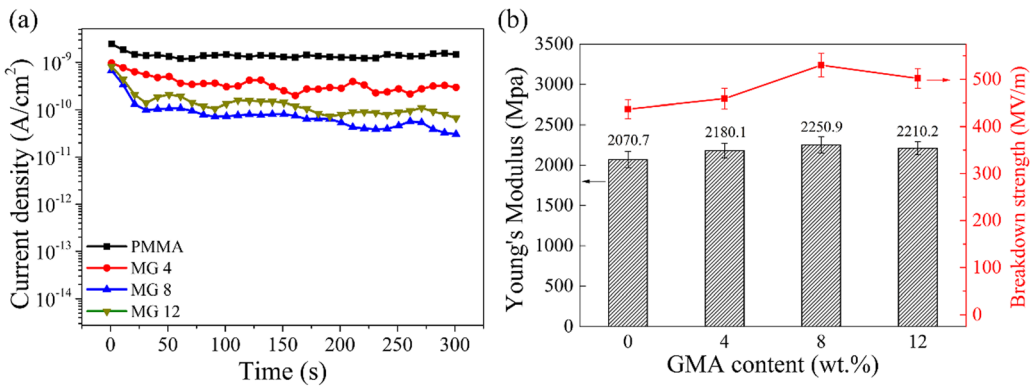

Fig. 6 Leakage current density under an electric field of 100 MV m^{-1} (a) and Young's modulus (b) of the PMMA and MG films.

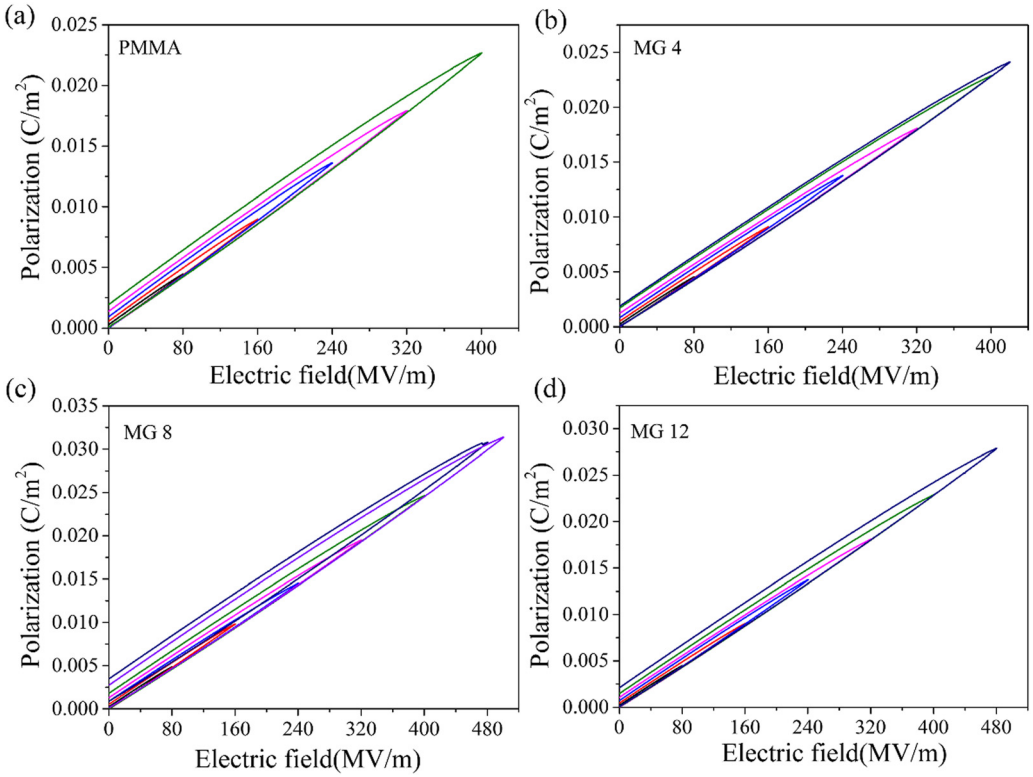

Fig. 7 *P–E* loops of the (a) PMMA, (b) MG4, (c) MG8, and (d) MG12 films.

In Fig. 5b, the E_b of MG 8 reached 530 MV m^{-1} at room temperature, which was an increase of almost 24% compared with the pristine PMMA film (437 MV m^{-1}). In addition, β also increased from 17.2 for the pure PMMA film to 27.4 for the MG 8 film, suggesting a better dielectric reliability compared with the pristine PMMA film. However, for the MG12 sample, it could be clearly found that the breakdown strength decreased from 530 MV m^{-1} for MG8 to 502 MV m^{-1} for MG12, which could be attributed to the increase in leakage current for the MG copolymers with a higher GMA content (see Fig. 6a).

It should be noted that the leakage current density is always utilized as a measure of the dielectric and energy storage performances in the case of high electric fields due to the electric field-dependent loss mechanisms in practical applications. The leakage current density of the PMMA and MG films was tested under a 100 MV m^{-1} field at room temperature. As shown in Fig. 6a, the introduction of GMA decreased the leakage current from 1.48 $\times$ 10^{-9} A cm^{-2} for the pristine PMMA film to 3.04 $\times$ 10^{-11} A cm^{-2} for the MG8 film, which was approximately two orders of magnitude lower than the pristine PMMA. According to previous research, hopping conduction between the charge traps is a typical conduction mechanism in organic materials. The introduction of larger GMA molecules can act as deep energy traps for the electrons, leading to a large residence time for the charge carrier and weak local electric field. Therefore, the copolymerization of GMA suppressed the electrical conduction of MG and the MG films displayed a lower leakage current density,[31,32] which was in accordance with the results for the dielectric loss at low frequency. As for the MG 12 film, a slightly increased leakage current of 6.66 $\times$ 10^{-11} A cm^{-2} could be found in Fig. 6a. Here, the higher GMA content increased the distance between the MG chains and decreased the motion resistance of the charges; therefore, the leakage current was improved for MG 12, which also corresponded to the trend for the breakdown strength.

The Young's modulus of a material also determines the electromechanical failure caused by mutual Coulombic force from the opposite electrodes under an applied field. The formula can be defined as $E_b = 0.606Y/K\varepsilon_{01/2}$, where Y is the Young's modulus and ε_0 represents the permittivity of free space,[33,34] which implies a higher Young's modulus is favorable for a higher dielectric breakdown strength. Fig. 6b represents the values of Young's modulus for the PMMA and MG films with different GMA contents. It can be seen clearly that the MG films had a higher modulus than the pristine PMMA film. For example, the highest Young's modulus was 2250 $\pm$ 100 MPa for the MG8 film compared with 2070 $\pm$ 90 MPa for the PMMA film. Therefore, both the leakage current density and Young's modulus results contributed to the enhancement of the dielectric breakdown strength of the MG films.

Energy storage properties

The unipolar P–*E* loops in Fig. 7 were used to investigate the *P–E* hysteresis behaviors of the PMMA and MG films. It could be found that all the films showed slim linear *P–E* loops and low remnant polarization. Compared with the pristine PMMA film, the MG films displayed higher polarization. For instance, the polarization increased from 0.023 C m^{-2} for the PMMA film to 0.032 C m^{-2} for the MG8 film, which represents an increase

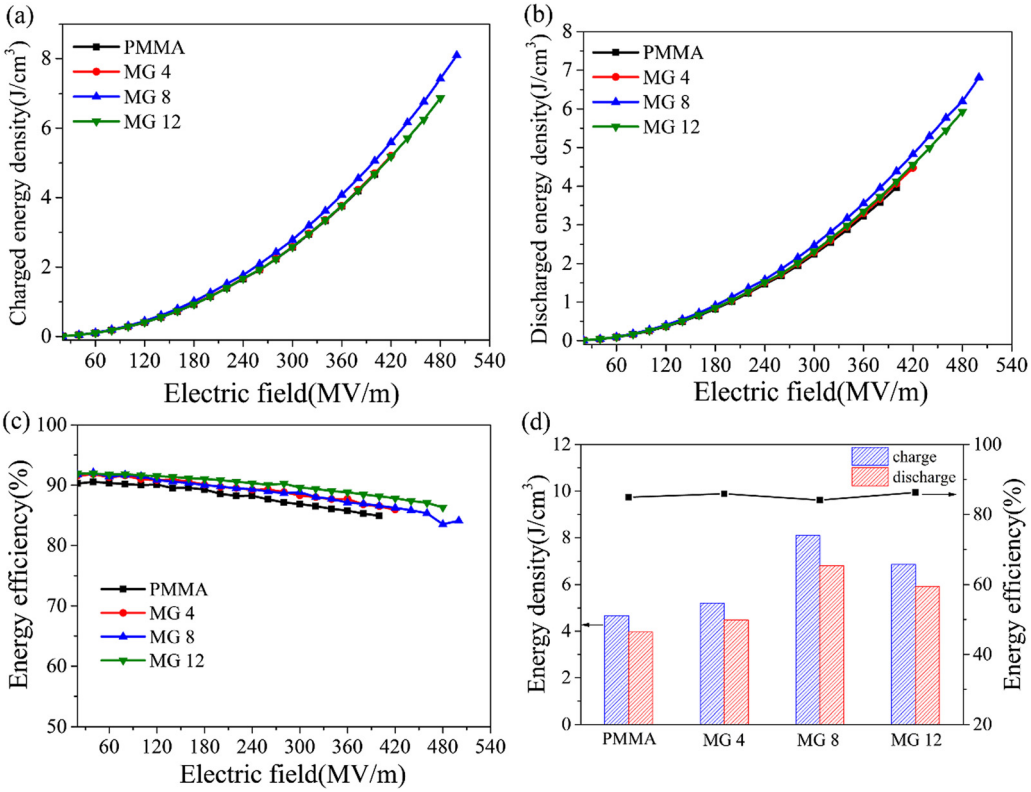

Fig. 8 Charged energy density (a), discharged energy density (b), efficiency (c), and relative values (d) of the PMMA and MG films.

of approximately 39%. Furthermore, the MG 8 film retained a similar remnant polarization of 0.003 C m^{-2} as the 0.002 C m^{-2} of the PMMA film. At the same time, the MG films displayed a higher breakdown strength than the PMMA film. Therefore, the increased polarity of GMA copolymerization improved the polarization ability of MG, and the concurrent effect of suppressed leakage current density and enhanced Young's modulus was due to the existence of GMA, thus boosting the higher breakdown strength of MG. All these factors are beneficial to achieve high energy storage for the MG films.

The energy density of the dielectric films could be calculated according to the *P*–*E* loops in Fig. 8. As expected from the above discussion, it can be clearly seen in Fig. 8a that the MG 8 film had the highest charged energy density, namely 8.10 J cm^{-3}, which represented a 73% increase compared with the 4.67 J cm^{-3} of the pristine PMMA. The stronger polarization, higher E_b, and low remnant polarization of the MG 8 film allowed it to achieve a high energy storage ability. Similar with the variation of the charged energy density, the MG 8 film in Fig. 8b showed the highest discharged energy density of 6.81 J cm^{-3}, which was 72% higher than that of the pristine PMMA (3.96 J cm^{-3}). In Fig. 8c, all the films had high charge–discharge efficiencies, and the difference between the films was very small. For example, the efficiency of the PMMA film was 84.9%, which was close to the 84.1% of the MG 8 film. The low dielectric loss and leakage current density of MG films are the essential reasons for their high charge–discharge efficiency. Fig. 8d displays the charge/discharge energy density and efficiency of the films when breakdown takes place, where it can be seen that the MG8 film showed the optimum energy storage properties.

The stability of dielectric membranes is very important for practical application. To evaluate the cycling performance of the films, a fast discharge test was employed repeatedly 30 000 times under 200 MV m^{-1}. As shown in Fig. 9, a stable discharge energy density of 1.19 J cm^{-3} was achieved for MG 8 compared with that of 0.51 J cm^{-3} for BOPP and 0.93 J cm^{-3} for PMMA under 200 MV m^{-1}, which therefore represented an increase of approximately 133% over that of BOPP. In addition, the discharge energy density showed no evident variation during the cycle test process, which further proved the excellent cycling

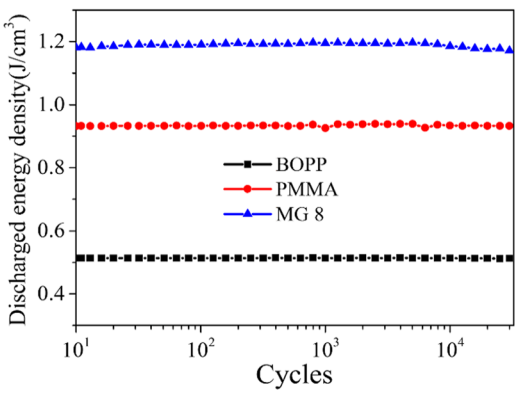

Fig. 9 Cyclic performance of BOPP, PMMA, and MG8 films.

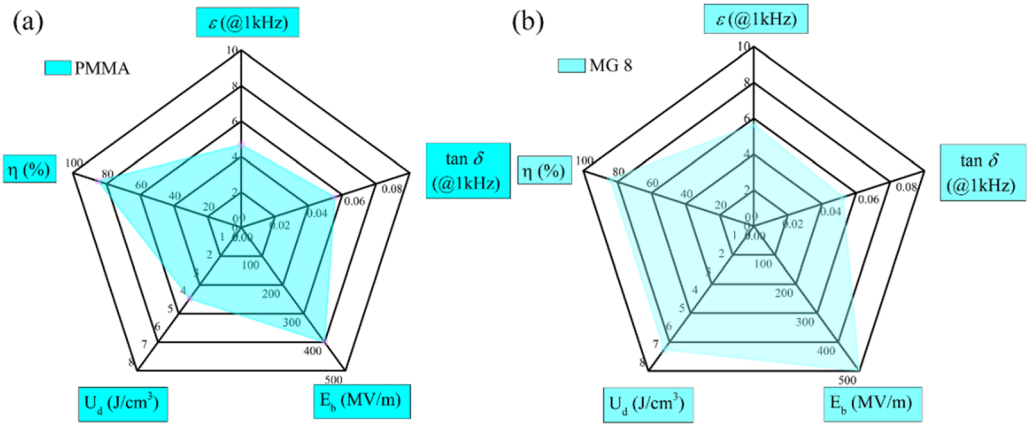

Fig. 10 Radar plots of the PMMA (a) and MG8 (b) films for comparison.

stability of the MG 8 film, owing to its low dielectric loss and leakage current density.

Radar plots of the PMMA and MG8 copolymer are given in Fig. 10, which allow the visual comparisons of ε, tan δ, E_b, U_d, and η for the films in order to assess their dielectric and energy storage properties. Among the radar plots, lager areas were obtained for the MG8 film in all areas except for tan δ. The radar images proved the copolymerization of GMA not only improved the permittivity, breakdown strength, discharge energy density, and energy efficiency, but also decreased the loss. Therefore, the comprehensive energy storage performances of the MG8 film were better than those of the neat PMMA film.

Finally, we compared the discharge energy density of a range of pure polymer substrates and their breakdown field strengths, as shown in Fig. 11. Different polymer substrates have been widely reported in recent years and these fall into two main categories: linear and ferroelectric. Although most of the linear polymers are capable of high electric fields, their discharge energy density is still somewhat low due to their poor dielectric constant. For ferroelectric polymers, their inherent dipole coupling properties also limit their use to a certain extent at high fields. In this paper, the MG8 copolymer achieved a discharge energy density of 6.8 J cm^{-3} in only intermediate electric fields, which exceeds the performance of most linear polymers, and it also demonstrated a good energy efficiency. The low cost of preparation and the ease of production means that it offers the possibility for supporting the later mass production of dielectrics.

Conclusions

In summary, methyl methacrylate (MMA) and glycidyl methacrylate (GMA) copolymers (MG) were successfully synthesized with varied MMA/GMA ratios. ^{1}H NMR and FTIR results demonstrated the successful preparation of MG. The strong polarity of GMA endowed a higher permittivity for MG, while the deep energy traps induced by GMA ensured a low dielectric loss and decreased leakage current density for the MG films. Consequently, a stronger dielectric breakdown strength of 500 MV m^{-1} was achieved for the MG 8 film compared with the 400 MV m^{-1} of the pristine PMMA

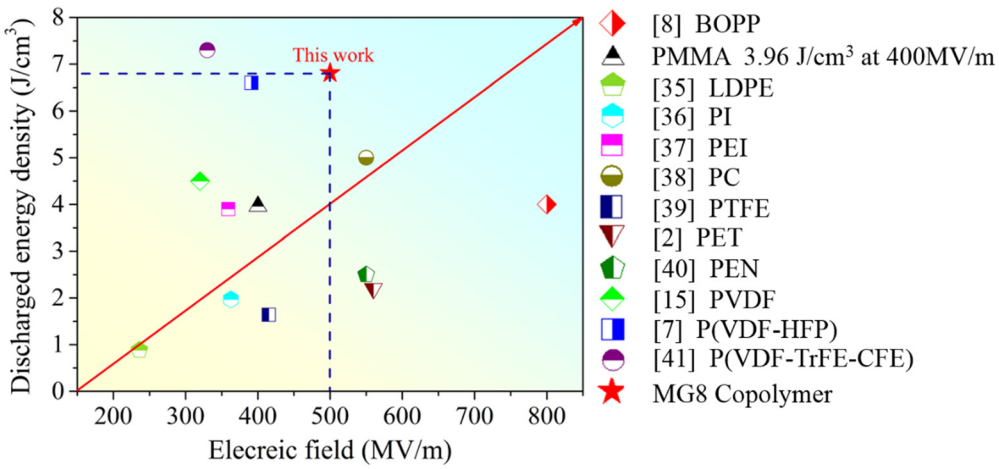

Fig. 11 Comparison of the discharged energy density and electric field in this work and other pure polymer dielectrics reported in recent studies.[2,7,8,15,35–41]

film. Hence, a highest discharged energy density of 6.81 J cm^{-3} and 84.1% charge–discharge efficiency were realized in a 500 MV m^{-1} electrical field. Furthermore, the low dielectric loss and leakage current density resulted in good cycling stability of the MG 8 film. This research presents a new linear dielectric material, which not only can be produced in a large scale, but also offers good potential performance modification prospects due to its reactive activity.

Conflicts of interest

The authors declare no conflict of interest.

Acknowledgements

This work is supported by the National Natural Science Foundation of China (No. 51273025), Jilin Provincial Science & Technology Department (20170203010GX) and the Education Department of Jilin Province (JJKH20170551KJ).

References

1 L. Yang, X. Kong, F. Li, H. Hao, Z. Cheng, H. Liu, J. F. Li and S. Zhang, *Prog. Mater. Sci.*, 2018, **102**, 72–108.
2 Q. Chen, Y. Shen, S. Zhang and Q. M. Zhang, *Annu. Rev. Mater. Res.*, 2015, **45**, 433–458.
3 Q. Li and Q. Wang, *Chem. Phys.*, 2016, **217**, 1228–1244.
4 Q. Li, L. Chen, R. Matthew, S. Zhang, G. Zhang, H. Li, E. Iagodkine, A. Haque, L. Chen, T. Jackson and Q. Wang, *Nature*, 2015, **523**, 576–579.
5 N. Meng, X. Ren, G. Santagiuliana, L. Ventura and E. Bilotti, *Nat. Commun.*, 2019, **10**, 4535.
6 P. Wang, D. Zhou, H. Guo, W. Liu and A. Trukhanov, *J. Mater. Chem. A*, 2020, **8**, 11124–11132.
7 P. Wang, D. Zhou, J. Li, L. Pang, W. Liu, J. Su, C. Singh, S. Trukhanov and A. Trukhanov, *Nano Energy*, 2020, **78**, 105247.
8 T. Zhang, X. Zhao, C. Zhang, Y. Zhang and Q. Chen, *Chem. Eng. J.*, 2020, **408**, 127314.
9 F. Wen, L. Zhang, P. Wang, L. Li, J. Chen, C. Chen, W. Wu, G. Wang and S. Zhang, *J. Mater. Chem. A*, 2020, **8**, 15122–15129.
10 E. J. Barshaw, J. White, M. J. Chait, J. B. Cornette and M. Rabuffi, *IEEE Trans. Magn.*, 2006, **43**, 223–225.
11 X. Yuan and T. Chung, *Appl. Phys. Lett.*, 2011, **98**, 20.
12 G. Zhang, H. Li, M. Antensteiner and T. Chung, *Macromolecules*, 2015, **48**, 2925–2934.
13 Y. Wang, L. Wang, Q. Yuan, J. Chen, Y. Niu, X. Xu, Y. Cheng, B. Yao, Q. Wang and H. Wang, *Nano Energy*, 2017, **44**, 364–370.
14 X. Zhao, J. Xie, J. Hu, Y. Liu, S. Sun and S. Song, *Mater. Today Commun.*, 2021, **29**, 102845.
15 S. Song, S. Xia, Y. Liu, X. Lv and S. Sun, *Chem. Eng. J.*, 2020, **384**, 123365.
16 F. Guan, J. Wang, J. Pan, Q. Wang and L. Zhu, *Macromolecules*, 2010, **43**, 6739–6748.
17 K. Yu, Y. Niu, Y. Zhou, Y. Bai and H. Wang, *J. Am. Ceram. Soc.*, 2013, **96**, 2519–2524.
18 L. Yang, X. Li, E. Allahyarov, P. L. Taylor and L. Zhu, *Polymer*, 2013, **54**, 1709–1728.
19 L. Zhu, *J. Phys. Chem. Lett.*, 2014, **5**, 3677–3687.
20 Y. D. Tang, W. H. Xu, S. Niu, Z. C. Zhang, Y. H. Zhang and Z. H. Jiang, *J. Mater. Chem. A*, 2021, **9**, 10000–10011.
21 C. Y. Xing, M. M. Zhao, L. P. Zhao and Y. J. Li, *Polym. Chem.*, 2013, **4**, 5726–5734.
22 G. Ru, H. Luo, X. F. Zhou, Z. H. Shen and D. Zhang, *J. Mater. Chem. A*, 2021, **9**, 27660–27671.
23 S. Xing, Z. B. Pan, J. J. Liu and J. W. Zhai, *J. Mater. Chem. C*, 2020, **8**, 12607–12614.
24 S. Gross, D. Camozzo, V. Noto, L. Armelao and E. Tondello, *Eur. Polym. J.*, 2007, **43**, 673–696.
25 M. Meunier, N. Quirke and A. Aslanides, *J. Chem. Phys.*, 2001, **115**, 2876–2881.
26 X. Lu, X. Zou, J. Shen, L. Zhang, L. Jin and Z. Cheng, *Nano Energy*, 2020, **70**, 104551.
27 M. Zhu, X. Huang, K. Yang, X. Zhai, J. Zhang, J. He and P. Jiang, *ACS Appl. Mater. Interfaces*, 2014, **6**, 19644–19654.
28 Y. Wang, X. Huang, T. Li, Z. Wang, L. Li, X. Guo and P. Jiang, *J. Mater. Chem. A*, 2017, **5**, 20737–20746.
29 S. Sun, Z. Shi, L. Sun, L. Liang, D. Dastan, B. He, H. Wang, M. Huang and R. Fan, *ACS Appl. Mater. Interfaces*, 2021, **13**, 27522–27532.
30 L. Sun, Z. Shi, B. He, H. Wang and H. Wang, *Adv. Funct. Mater.*, 2021, **31**, 2100280.
31 Y. Zhou, C. Yuan, S. Wang, Y. Zhu and Q. Li, *Energy Stor. Mater.*, 2020, **28**, 255–263.
32 C. Q. Li, J. W. Zha, H. Q. Long, S. J. Wang, D. L. Zhang and Z. M. Dang, *Compos. Sci. Technol.*, 2017, **153**, 111–118.
33 Q. Li, G. Zhang, F. Liu, K. Han, M. R. Gadinski, C. Xiong and Q. Wang, *Energy Environ. Sci.*, 2015, **8**, 922–931.
34 K. Stark and C. Garton, *Nature*, 1955, **176**, 1225–1226.
35 X. C. Zhao, Y. J. Bi, J. H. Xie, J. Hu, S. L. Sun and S. X. Song, *Polym. Test.*, 2021, **95**, 107094.
36 Q. K. Feng, Q. Dong, D. L. Zhang, J. Y. Pei and Z. M. Dang, *Compos. Sci. Technol.*, 2022, **218**, 109193.
37 R. Qiao, C. Wang, S. Chen, G. H. He, Z. J. Liu, H. Luo and D. Zhang, *Composites, Part A*, 2022, **152**, 106679.
38 G. Liu, Y. Feng, T. D. Zhang, Q. G. Chi and Q. Q. Lei, *J. Mater. Chem. A*, 2021, **9**, 16384.
39 S. B. Luo, T. Q. Ansari, J. Y. Yu, L. Q. Cao, H. T. Huang and R. Sun, *Chem. Eng. J.*, 2021, **412**, 128476.
40 M. Rabuffi and G. Picci, *IEEE Trans. Plasma Sci.*, 2002, **30**, 1939.
41 C. Chen, J. W. Xing, Y. Cui, T. D. Zhang, Q. G. Chi, X. Wang and Q. Q. Lei, *J. Phys. Chem. C*, 2020, **124**, 5920–5927.